FLUX DENSITY MEASUREMENT ON LARGE-SCALE RECEIVERS

Marc Röger[1], Patrik Herrmann[2], Miriam Ebert[1], Christoph Prahl[1], Steffen Ulmer[1], Felix Göhring[3]

[1] German Aerospace Center (DLR), Solar Research, Plataforma Solar de Almería, 04200 Tabernas, Spain

Phone: +34-950259806, E-Mail: marc.roeger@dlr.de.

[2] Technical University of Darmstadt, Reactive Flows and Diagnostics, Germany

[3] German Aerospace Center (DLR), Solar Research, Cologne, Germany

Abstract

Commercial solar tower plants have much larger aperture surfaces than the receiver prototypes tested in earlier R&D projects. Existing methods to measure the solar flux density in the receiver aperture face new challenges regarding the receiver size. Also, the requirements regarding costs, accuracy, spatial resolution, and measuring speed are different. Flux density measurement delivers the spatial distribution of the concentrated solar radiation on a receiver aperture, measures receiver input power, and monitors and might control heliostat aimpoints. This paper resumes existent concepts, presents new ones and evaluates them against a catalogue of requirements. Direct and indirect moving bar techniques offer high measurement accuracy, but also have the disadvantage of large moving parts on a solar tower. In the case of external receivers, measuring directly on receiver surfaces avoids moving parts and allows continuous measurement, but is not as precise. This promising technique requires, due to specific reflectance properties of current receiver materials, proper scientific evaluation. Measurement-supported simulation techniques can also be applied to cavity receivers without installing moving parts. They have reasonable uncertainties under ideal conditions and require comparatively low effort.

Keywords: flux density measurement, receiver input power, central receiver system, solar tower

1. Introduction

Flux density measurement on large-scale receivers is an important issue, because this technique delivers the receiver input power which is necessary to get performance figures of the receiver and heliostat field. Moreover, continuous measurement of the flux density distribution facilitates efficient receiver operation and heliostat aimpoint control. Different receiver types and different requirements regarding the measurement purpose result in several possible solutions for flux measurement on large-scale receivers.

We distinguish two basic receiver types: external receivers where the absorber surface is more or less equal to the aperture surface, and cavity receivers, where the aperture is not identical to the absorber surfaces. In the first case, the external receiver surface may be used as a measurement target. In the second case, the flux density in the aperture surface must be measured in a different way because the absorber surfaces are inside the receiver cavity.

The different measurement techniques can be classified in indirect, direct and measurement-supported simulation methods. While indirect methods use CCD cameras to measure the solar radiation reflected off a surface, the direct methods use flux sensors which directly deliver a measurement signal proportional to the irradiative flux. Simulation methods may also be used to get highly-resolved solar flux maps. The authors recommend supporting the simulations by either direct or indirect simplified measurement methods, which serve as validation of the simulations and hence can be reduced in resolution and complexity.

2. Flux density measurement techniques

This section presents existent concepts and new developments to measure the flux density distribution on large-scale receivers of central receiver systems.

2.1. Flux density measurement by using a white diffuse moving bar target and CCD camera

This indirect method uses a white, diffusely reflecting target which is moved directly in front of the absorber surface. A CCD camera takes a series of photos [1, 2]. Then, in each image, the target region is cropped by an image processing algorithm and combined to a surface covering the whole region of interest. The intensity of reflected solar light is calibrated by using a radiometer which is mounted directly behind the moving bar plane. Figure 1 gives an overview of the ProHERMES measurement system [2]. This measurement method can be applied to a variety of different receiver types. It was successfully used in various characterizations of smaller R&D prototypes.

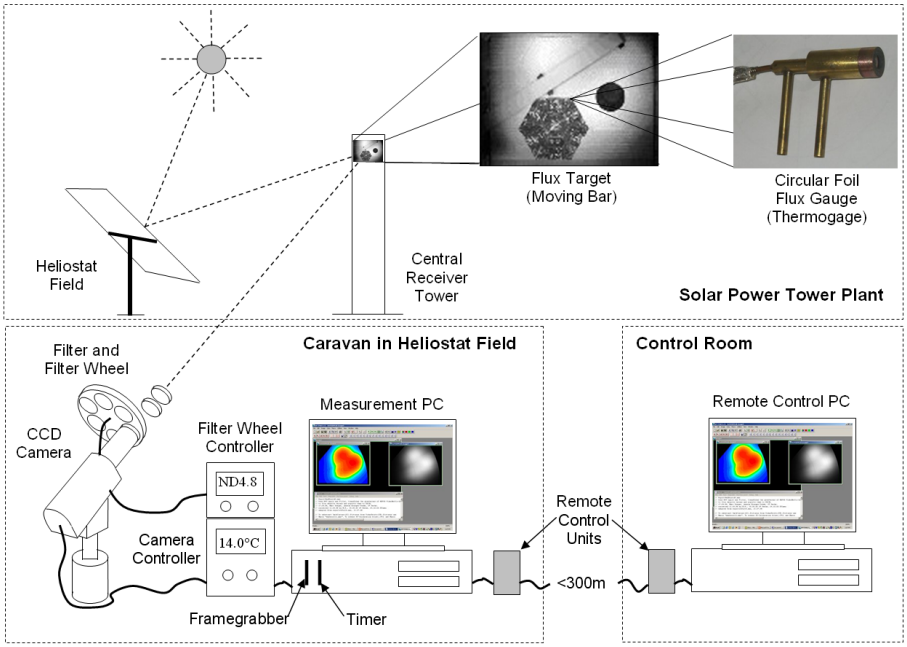

Fig. 1. Overview of ProHERMES measurement systems [3]

Figure 2 gives an overview of different moving mechanisms. Rotating moving bars are a good choice for small-scale prototype receivers, because only one drive is necessary at the rotating axis which results only in one small opening in the front protection of the tower. The upscaling of rotational moving bars which rotates around a pivot as used in the ProHERMES setup is critical because of high angular momentums.

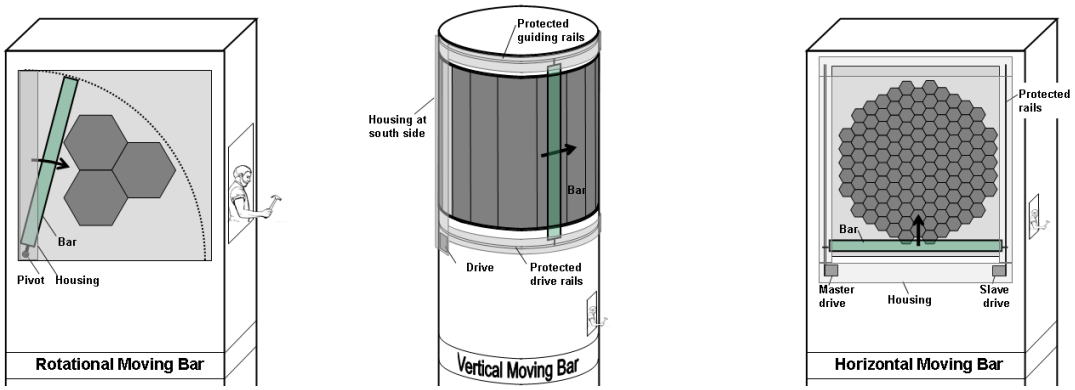

Fig. 2. Possible mechanisms of moving bars

However, upscaling should be possible by switching over to a concept with linear movement of the moving bar. Issues of thermal expansion and thermal load by convection of hot air and radiation have to be considered in the design process. External surround receiver may be equipped preferably by vertical linear moving bars, which are moved along the circumferential receiver line. The drive should be located at the lower part of the receiver with sufficient distance and protection from concentrated solar radiation to avoid

the exposure to hot convection air flows. The upper part may only be guided in a rail or rod to avoid temperature sensitive drives and motors on this region. Depending on the angle of acceptance of the receiver, several cameras are needed on ground, or alternatively, a single moving camera, mounted on the lower end of the moving bar.

In the case of cavity receivers, usually there is space on both sides of the receiver to mount guiding rails. Then, a horizontal linear moving bar with two motors operated in master/slave configuration is a feasible option. The two drives and rails are out of the high-solar-flux regions and areas with hot air convection and can be protected adequately against the lower solar fluxes. Master/slave operation helps to avoid tilting of the moving bar.

For all systems, measurement accuracy should be comparable to the ProHERMES system. Having corrected systematic uncertainties, total measurement is very good, being in the range from -4.7% to +4.1% [3, 4]. The highest contribution to uncertainty is caused by uncertainties of calibration of the radiometer (about ±3%). Further relevant uncertainties to measurement of flux density distribution on the receiver aperture plane are the distance between the measurement plane and aperture plane in interest, spectral effects and uncertainties in positioning and sizing during image processing. The control of the degradation of the radiometer paint and the Lambertian surface of the moving bar and calibration from time to time is regarded as indispensible for maintaining a high measurement accuracy.

2.2. Flux density measurement on external receiver surfaces using a CCD camera

This indirect method uses flux sensors and calibrated CCD camera images similar to section 2.1, but the receiver surface is utilized as measurement target. An additional moving bar is not required. Requirements are that the surface reflects more or less diffusely, i.e. not specularly and that there is no pronounced height profile of the receiver surface.

A spectral filter reduces the effect of emitted thermal radiation of the receiver which would bias the signal of reflected solar radiation on the CCD camera chip. By cutting off radiation with wavelengths above 0.6 μm, the measurement uncertainty caused by this effect can be reduced from 0.8% to below 0.1% (absorber surface temperature 1200°C, emissivity 0.9, 500 suns, camera Pike F100B). For lower temperatures or higher solar concentrations, no filter is necessary.

Figure 3 (a1) shows a grabbed CCD image of an open volumetric receiver tested at the Plataforma Solar de Almería (PSA). The gray value image shown in Fig. 3 (a2) was rectified and the gaps in between the receiver cups are cut out and interpolated from adjacent pixels. As reflectivity of receiver surfaces is usually not homogeneous, we see significant differences of the light reflected off different receiver cups. A correction matrix to correct spatial variations in local hemispherical reflectance must be applied. To get this matrix, the receiver surface has to be illuminated homogeneously or with a known flux distribution. Authors worked with ambient light at different meteorological conditions (clouds). Artificial illumination with a known luminosity profile of a stage projector or beamer would be another option. After this correction, the scattering due to inhomogeneous cup reflectivity has been reduced significantly; see Fig. 3 (a3). Although, some minor artifacts are visible. These might be caused by varying individual receiver cup reflectivity over time and non-proper cut out of the gaps between the receiver cups.

Assuming a constant bidirectional reflectance distribution function (BRDF), i.e., a perfect diffusely reflecting material, the corrected gray value distribution can be calibrated using a water-cooled Gardon flux gauge. In the tests, it was demonstrated that using more than one flux gauge enhances measurement accuracy, because the non-ideally, non-homogeneously reflecting receiver surface increases errors. Calibrating translates the gray value scale to flux density scale (kW/m^2). Comparing Fig. 3 (a3) with the reference moving bar measurement (b) shows an acceptable agreement, having in mind that the moving bar measures in front of the receiver plane (flux distribution changes) and a focus usually slightly changes during moving bar measurement due to tracking heliostats and wind.

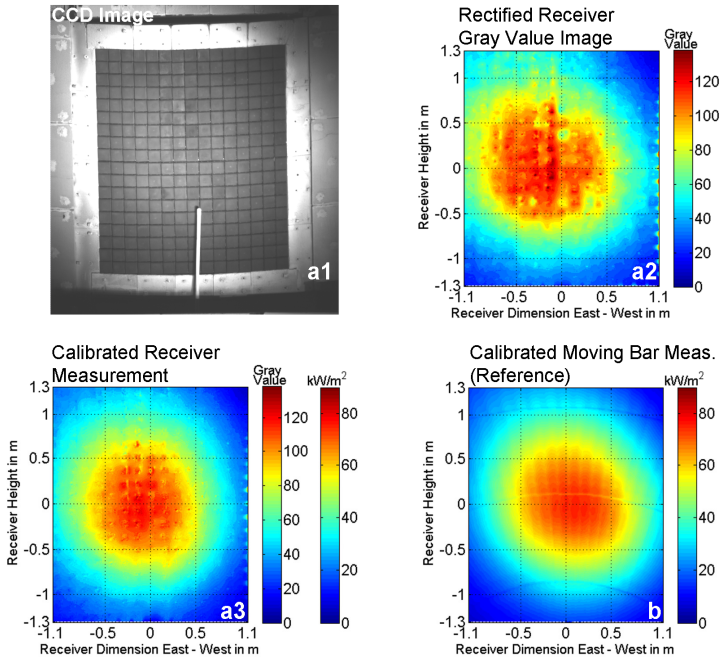

Fig. 3. Grabbed CCD image (a1), rectified gray value image in false colours (a2), image after application of brightness correction matrix (a3). Image (a3) also shows the colour bar after calibration, neglecting angle dependence of reflection on receiver. Image (b) shows the moving bar measurement as reference (Test open volumetric receiver PSA, ~225 kW, 13.12.07, 13:20h).

The assumption of a constant BRDF is only correct for specific angles between receiver, camera and heliostat, and hence is only an approximation. The reflectivity of real receiver surfaces often depends on the ray incidence angle and camera observation angle. For this reason, the receiver material was characterized in a gonioreflectometer with a light source at a zenith angle of 14°. The sketch inside Fig. 4 shows the configuration of measurement. Fig. 4 shows the variation of the normalized BRDF depending on sensor zenith angle and azimuth angle. Unfortunately, the region of zenith angles between approximately 0 to 20° could not be measured, because the light source partly or totally blocked the sensor. However, we can observe an increase in the BRDF values around this region which indicates a partly retro-reflective behavior.

A solar gonioreflectometer experiment series was performed at the CESA-1 tower at the PSA. Assuming Helmholtz reciprocity, the sensor can be exchanged by the camera. For a solar field, this means that the light source position (different heliostat) varies, while the sensor position (camera) is fixed. The camera was positioned at the end of the heliostat field to have free sight to the receiver and not too many nearby heliostats. Groups of heliostats having different angles to the receiver surface were focused subsequently while during each configuration, CCD images of the receiver surface and moving bar measurements were performed. The ratio of receiver surface brightness (after application of the brightness correction matrix) and brightness of moving bar measurement can be regarded as a normalized BRDF value for the specific configuration. The measurements are also plotted with full markers in Fig. 4. Being a field test, we can observe a good agreement with the laboratory gonioreflectometer measurements.

Indeed, we also observe that heliostats near the camera position (zenith angle around 10° and azimuth angle around 180°) have a high BRDF value which exceeds the mean almost by 50%. This means that measuring the light reflected off the receiver coming from these heliostats, is overestimated compared to heliostats which are located at zones with lower BRDF values. Figure 5 shows a map of the CESA-1 heliostat field with isolines of azimuth and zenith angles projected in the heliostat plane. The map is valid for a plane receiver, inclined 30° to the vertical at 84 m height above ground, and the camera placed at the end of the field. The heliostats are colored by their individual normalized BRDF. The values are taken from the laboratory gonioreflectometer measurements of Fig. 4. Heliostats directly nearby the camera are not colored because of lack of measurement data, but one can observe that light from heliostats in the region close to the

camera is overestimated while light from heliostats near the tower is underestimated. Also, a lot of heliostats represent a mean value and are measured correctly. Consequently, a fixed calibration constant as in the procedure of Fig. 3 may be used, if a lot of heliostats, which levels out differences, are used and only approximate flux values are needed. However, for higher accuracies, the authors recommend to consider this effect. It can be reduced by placing the camera close to the tower and looking upwards, if view of sight permits this. In this case, the camera would not be placed directly in the region which is affected by the retro-reflective peak. This was done during tests at the Solar Tower Jülich [5]. Additionally, different calibration constants could be applied, depending on which groups of heliostats reflect how much radiation. Generally speaking, this is a challenging task, because external receivers usually are cylindrical and not plane, so one heliostat may have different angles of incidence on the receiver. Further details about this measurement principle and more gonioreflectometer measurements are found in [5].

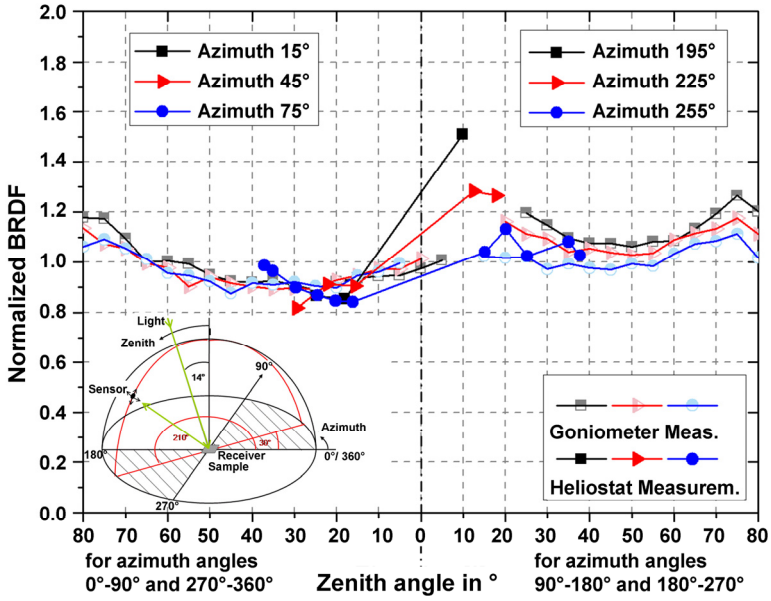

Fig. 4. Normalized BRDF values of a volumetric ceramic receiver as a function of zenith and azimuth angle. Comparison of laboratory gonioreflectometer measurements (sketch left and half markers) and measurements done with heliostat groups of solar field (full markers, also see Fig. 5).

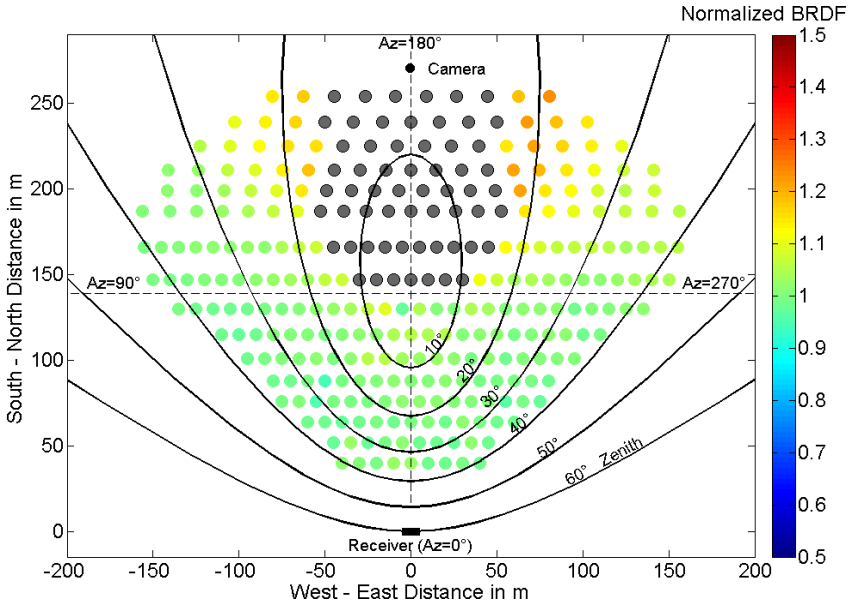

Fig. 5. Normalized BRDF values for each heliostat of the CESA-1 heliostat field at PSA, assuming a plane volumetric air receiver at 80 m height, 30° inclined and camera position at the end of the field.

2.3. Flux density measurement by using a stationary stripe-shaped target and moving focus

This indirect method was first mentioned in [6]. Instead of stripe-shaped moving target, the target is fixed, preferably directly above or on the west side of the receiver and the focus is swept over this white target in steps. The target is stripe-shaped and not squared to reduce wind forces and material costs. It is preferably mounted on the west side of the receiver because of two reasons: Heliostats and the sun move from east to west over the day. Hence, the effect of focus variation due to spatial shift of aimpoint and due to time passed during measurement compensate partly for a target on the west side. A second reason is that if there is any backlash in the gearbox, it has no influence while the heliostat maintains the tracking direction. The bar has to be mounted in a distance to the aperture so that there is no illumination of the target in normal receiver operation to avoid measuring radiation several times. Figure 5 visualizes the procedure.

Moving the whole focus over the target as proposed in [6] would stop receiver operation totally and require an actively cooled target. Hence, we suggest splitting up the focus in various heliostat groups. For example, 80% still tracks on the receiver, and 20% is swept over the target in various steps. A CCD image is taken, when the slowest (i.e. usually the nearest) heliostat has reached its new aimpoint. Then, the aimpoint is moved further to take the next image. After the scan of these heliostat groups, the images are assembled together. Before assembling, slight solar irradiation variations during the scan are compensated by weighting each stripe with a DNI value normalized with the DNI during the first image. A flux sensor reading calibrates the resulting gray value distribution. After evaluating all the heliostat groups, the flux images are added up to get the final result.

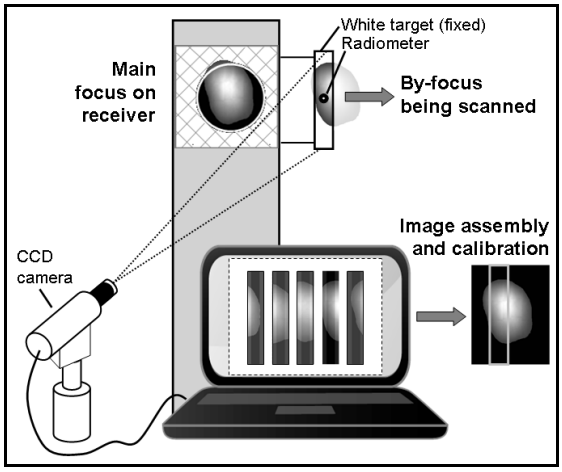

Fig. 5. Procedure of scanning part of the focus over a stripe-shaped, fixed target.

The effects of focus variation due to spatial shift of aimpoint and due to time passed during measurement were evaluated by raytracing simulations. The focus variation due to spatial shift of the aimpoint is mainly caused by changes in cosine losses and optical aberration. The focus variation, caused by the approximately six minutes needed to perform five scans, is due to the varying sun angles and heliostat orientations, leading also to varying cosine losses and optical aberrations. Both variations are minimum at solar noon and maximum in the evening and the morning. For a bar target mounted at the west of the tower, these effects compensate to some extent. At the CESA-1 plant in Almería at 8:00h at the morning, the uncertainty in the solar flux distribution due to focus variation by spatial shift of aimpoint and time is 1.2%, and the uncertainty in integrated power 0.5%.

The measurement uncertainties of CCD camera and target are the same as for the PROHERMES system (see section 2.1). A further, important issue is the accuracy of heliostat tracking and the number of heliostats involved. If tracking errors were too high, the step size in aimpoint shift would not be equal, and the individual images could not be assembled totally correctly. However, if there are a lot of heliostats involved, then this error compensates to a great extent. In a simulation study it is shown that with 120 heliostats having a normally distributed tracking error of 0.65 mrad for each axis, a total measurement uncertainty in the range from -6.0% to +5.5% can be reached. If the tracking error was 1.6 mrad for each axis, measurement

uncertainty would increase up to -9.1 to +8.8%. The uncertainty in integrated power is estimated to -4.3 to +3.6%. Measurements with individual heliostats were done and a stripe assembling algorithm has been developed so far.

2.4. Flux density measurement by using a moving bar with mounted sensors

This direct method also uses a moving bar, either rotational or linear, on which sensors are mounted. These sensors scan the aperture surface while moving the bar over the focus. The disadvantage of Gardon flux gauges is that these are thermal sensors and hence have a high response time. The scan would take several minutes, resulting in the necessity of active water cooling of moving bar and sensors. New thin film heat flux sensors as used in the MDF system can be used [7]. They have fast time constants in the range of µs and allow a rapid scan without water cooling. The tests with this system reported in [7] were promising.

Being a direct measurement method, uncertainties caused by camera and target properties are avoided. Nevertheless, also a moving bar is necessary and the sensor cables have to be routed from the moving bar to a data acquisition system.

2.5. Flux density measurement by using stationary sensors

Moving parts are avoided, if several water-cooled flux gauges are distributed in the aperture plane or on the receiver surface. Heat flux maps are created by interpolation between the measurement points. Numerous sensors are required to get accurate results. Non-equal sensor distribution over the measurement surface allows the reduction of sensor number while maintaining a reasonable measurement uncertainty. Stationary sensors are used, for example, at the PS-10 plant in Seville [8]. As being a direct method, measurement accuracy at sensor locations is high, however, spatial resolution may only be moderate while not using excessive numbers of sensors.

2.6. Flux density measurement by measurement-supported simulation

State-of-the-art ray tracing codes allow a very accurate prediction of the solar flux on any surface. Accuracy of results depend mainly on the quality of input parameters, such as correct representation of concentrator contour errors (slope errors), heliostat tracking errors, heliostat positions and geometry (blocking and shading, cosine effects, optical aberration), mirror reflectivity, atmospheric conditions (DNI, sunshape, atmospheric attenuation), tower geometry (shading) and receiver position. However, the validity of simulation results should be confirmed by measurements, either by an indirect or direct method. These measurements may be reduced significantly in effort compared to the determination of solar flux by measurement only.

On the CESA-1 solar tower at the Plataforma Solar de Almería, a solar-hybrid gas turbine system was tested. Ray tracing simulation results of the tests were compared to flux maps produced with a moving target (see section 2.1). The raytracing code STRAL [9] was used. As input for the simulation, the heliostat contour errors were measured by deflectometry. The exact receiver position relative to the known heliostat field was measured by a tachymeter. A circumsolar ratio of 5% was assumed which is recommended as a single representative value [10]. The DNI was measured and used as input parameter. The final heliostat reflectivity was chosen in a way that the simulated and the measured solar flux on a radiometer mounted in the receiver area was the same. It was cross-checked with measured values and the deviations were below 2.8%, which is low compared to the uncertainties of DNI and reflectivity measurement, atmospheric extinction, and sunshape. A major issue was to use correct aimpoints in the simulations because the used version of the control software did not always work without errors. A random tracking error of having a sigma of about 0.9 mrad for each axis was applied. Fig. 6 (a1) shows the simulated flux distribution on the radiation shield plane. The black circle indicates the receiver aperture. It was simulated that 257 kW were intercepted by the aperture.

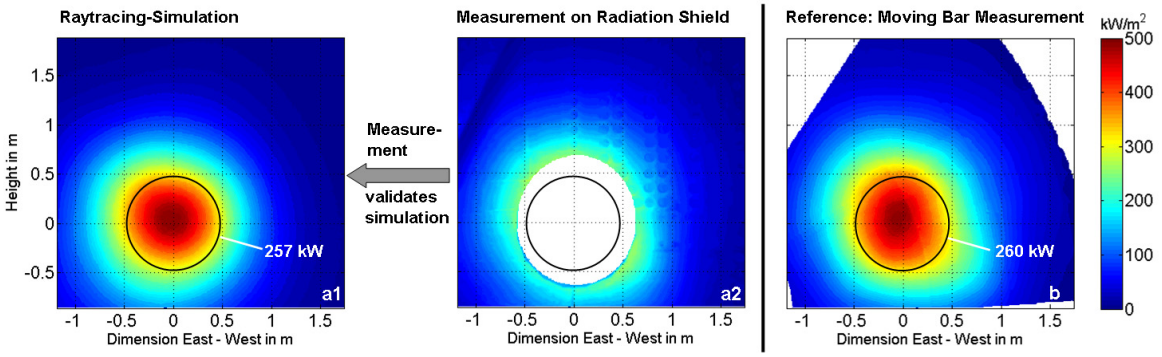

Fig. 6. Flux density distributions on radiation shield plane in kW/m^2.(a1) Raytracing Simulation. (a2) Measurement directly on radiation shield and after application of correction matrix and calibration. (b) Moving bar reference measurement. Test PSA, 46 Heliostats, 19.05.10, 12:50h

In order to see whether the simulation reflects reality, it was compared with an indirect flux measurement method, using a CCD camera and the white radiation shield mounted around the aperture surface as target, see Fig. 6 (a2). To correct spatial variations in local hemispherical reflectance on the radiation shield, a correction matrix was applied to the gray value images of the CCD camera, similar to the procedure described in section 2.2. The resulting image was calibrated by radiometers mounted in the measurement surface. The standard deviation between the simulated (a1) and measured flux distribution on the radiation shield (a2) is a measure for the quality of the simulation. Optimizing the simulations by correcting the global tracking offset for example, reduces this standard deviation. A standard deviation of 8 kW/m^2 was reached in the presented case.

Once confirmed a simulation, the flux can be evaluated on the aperture surface using the validated simulation. The quality of the flux distribution strongly depends on the uncertainty of aimpoints, i.e. the heliostat control system and heliostat tracking accuracy. However, in different experiments, it could be shown that despite the uncertainty in aimpoints, the solar input power into the aperture could be simulated with a low deviation in the range of 1 to 3% compared to a moving bar measurement.

Another possibility to validate the simulations is using distributed flux gauges in the receiver aperture, i.e., a direct method. Depending on the number of gauges and the uncertainty of aimpoints, this validation procedure is especially valuable for large-area receivers with multi-aimpoint strategy and relative small reflection shield surface around the receiver.

Indeed, comparing the flux distribution of the simulation result (a1) with the moving bar reference measurement (b), which normally is not available, we observe a satisfying agreement for the flux distribution and a good agreement for the intercepted power on the receiver aperture. The same is valid for the comparison between the measurement on the radiation shield (a2) and the moving bar reference (b), which indicates that a measurement on the radiation shield is suitable for this purpose.

3. Evaluation of concepts

Several requirements must be satisfied to reach the design specifications. The requirements are classified in three different categories with varying importance: necessary, targeted and nice-to-have requirements. The different concepts are compared based on these requirements.

3.1. Catalogue of requirements

Figure 7 shows a visualization of the catalogue of requirements. Necessary requirements must be fulfilled in order to be considered in the evaluation: Concepts must measure the desired quantity, must be scalable to large receivers, and must reach a high operational safety for the workers and sufficient temperature stability.

The targeted requirements should be fulfilled to a maximum, i.e., concepts should have a low measurement uncertainty and a high reliability and availability. Flux measurements purpose three main objectives which

not necessarily have to be complied with all at the same time. Tasks are the determination of solar flux distribution on the receiver surface and/or the integrated solar input power into the receiver aperture, e.g. for acceptance testing, and/or delivering input to an aimpoint control system. While the first two measurements may only be needed at some specific points in time, but with very high measurement accuracy, input for an aimpoint control system must be available continuously, but with lower accuracy. As a consequence, the concepts must be evaluated regarding their measurement objective individually. Besides a low measurement uncertainty and a high system reliability and availability, the system should have a low susceptibility to the expected loads and environmental conditions (e.g. wind, humidity, rain, dust etc.). The investment, maintenance and operating costs should be low. This can be reached e.g. by maximizing the use of standard parts which comply with the other mentioned requirements.

Nice-to-have requirements are considered optional. The technical complexity of the system should be low, ensuring an integral arrangement of the moving bar into the receiver system and should be easy to be operated. The development cost and time also should be modest.

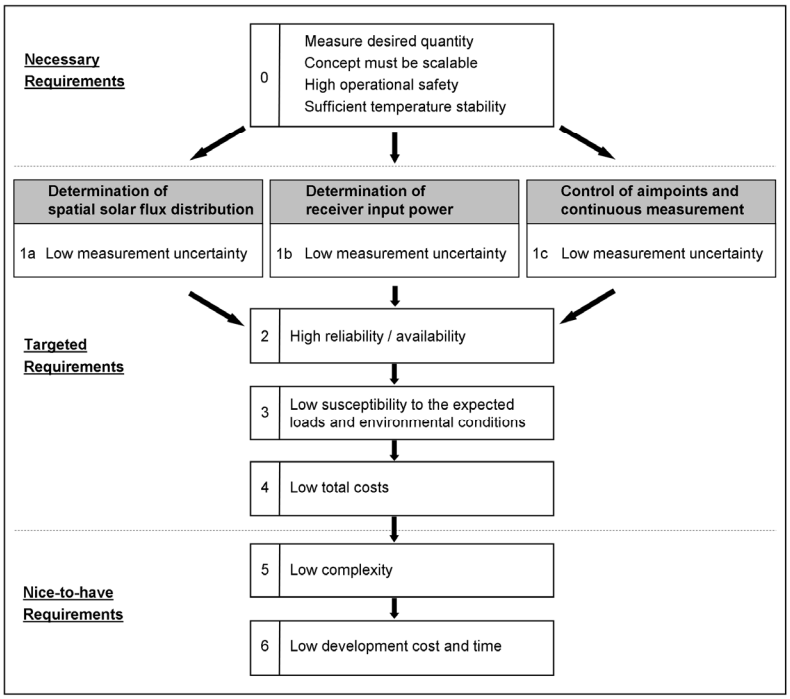

Fig. 7. Requirements to reach the design specifications. The fields marked in grey show the different measurement objectives.

3.2 Comparison of concepts

The different concepts are evaluated regarding the catalogue of requirements taking into account the three measurement objectives (1a) to (1c) of Fig. 7. Table 1 shows the scores for the individual requirements and the weighted sum. Necessary requirements must be fulfilled completely anyway, so that they don't appear in the table.

In the lower part of the table, the weighted sum is listed individually for each measurement objective (1a) to (1c) and one value for all measurement objectives. For the column "direct measurement with distributed stationary sensors (2.5)", two scores are given, depending on the numbers of sensors used. A higher sensor number increases measurement accuracy, but also increases the costs. For the columns of measurement-supported simulations (2.6 and 2.7) also two scores are listed. The first score assumes that the heliostat aimpoints are known with sufficient accuracy, i.e. a state-of-the art aimpoint control with good heliostats is installed. Then, the number of flux sensors (2.6) or the radiation shield measurement surface compared to the receiver surface (2.7) may be small while a low measurement uncertainty is guaranteed. The second score is given if the heliostat aimpoint system does not work properly. Then, the best simulation run out of runs with

different statistical aimpoint distributions would be chosen. For this, more flux sensors or a larger irradiated radiation shield surface would be needed.

	Moving Bar Technology		Technologies without Moving Bar				
Method	Indirect	Direct	Indirect	Indirect	Direct	Simulation - Indirect	Simulation - Direct
Short Description	Moving Bar Target CCD Camera	Moving Bar with Sensors	External Receiver Surface CCD Camera	Stationary Bar Target, Moving Focus CCD Camera	Distributed Stationary Sensors	Supported by Radiation Shield Meas. CCD Camera	Supported by Measurement with Sensors
Section	(2.1)	(2.4)	(2.2)	(2.3)	(2.5)	(2.6)	(2.6)
1 Low Measurement Uncertainty (Weight: 50)							
1a: Solar Flux Distribution	++	+	0	+	0/-[1]	+/0[2]	+/0[2]
1b: Receiver Input Power	++	++	+	+	+/0[1]	+/0[2]	+/+[2]
1c: Aimpoint Control	+	+	++	-	+/0[1]	+/0[2]	++/+[2]
2 High Availability/Reliability (Weight: 20)							
	+	+	++	+	+	++	++
3 Low susceptibility to Loads/Environment (Weight: 10)							
	0	0	+	+	+	+	+
4 Low Total Costs (Weight: 10)							
	0	0	++	+	0/+[1]	+/++[2]	0/+[2]
5 Low Complexity (Weight: 5)							
	+	+	++	++	0/+[1]	++	+
6 Low Development Cost and Time (Weight: 5)							
	+	+	+	0	+	+	+
→ Weighted Sum							
1a: Solar Flux Distribution	130	80	90	100	40/0	130/90	110/70
1b: Receiver Input Power	130	130	140	100	90/50	130/90	110/120
1c: Aimpoint Control	80	80	190	50	90/50	130/90	160/120
All: 1a – 1c	110	100	140	80	70/30	130/90	130/100

[1] using many / only few sensors
[2] with good / poor knowledge of heliostat aimpoints or with many / few measurement points

Table 1. Evaluation of different solar flux measurement techniques

A very suitable technique to measure the spatial solar flux distribution (measurement objective 1a in Fig. 7) is the moving bar technique with CCD camera (section 2.1). A linearly moving bar is evaluated as more feasible than a rotating bar for large-area receivers. Currently, a linear moving bar is designed. A further suitable technique for flux distributions is the measurement-supported simulation using distributed stationary flux sensors (section 2.6), assuming a state-of-the-art heliostat aimpoint system. Not recommended for measuring flux distributions on large-scale receivers is the technique to use distributed stationary sensors (section 2.5) only, because of the large numbers required to reach reasonable accuracy in interpolating between them. The other techniques are in the middle of the rankings.

The determination of the receiver input power (measurement objective 1b in Fig. 7) is done by integrating the solar flux distribution. Hence, local uncertainties in flux distribution frequently do not affect the integral strongly. Additionally to the moving bar technique with CCD camera (section 2.1) and the measurement-supported simulation using distributed stationary flux sensors (section 2.6) mentioned above, the moving bar

with sensors (section 2.4) and the measurement on external receiver surface (section 2.2), if applicable, are suitable for this task. The other techniques are in the middle of the rankings, depending on the particular conditions.

A well suitable measurement technique for aimpoint control measurements and continuous measurements (measurement objective 1c in Fig. 7) is measuring on the external receiver surface (section 2.2). It is obvious, that this technique is not applicable to cavity receivers. Not recommended for aimpoint control is the technique using a stationary bar target and a moving focus (section 2.3), because aimpoints are moved, measurement takes some minutes and receiver power is reduced. The other systems can all be used for aimpoint control, depending on the particular conditions.

4. Conclusion

In general, the direct and indirect moving bar techniques (sections 2.1 and 2.4) are attractive due to their low measurement uncertainty in all measurement tasks. However, the mechanical moving bar causes more costs and may have a higher susceptibility to loads and environment. The opposite occurs with the measurement on the external receiver surface (section 2.2). Here, we have higher measurement uncertainty for the flux distribution and decent accuracies in the other two tasks, but it is technologically simple. The technique using a stationary bar target and a moving focus (section 2.3) and the distributed stationary sensors technique (section 2.5) suffer from not in all measurement tasks sufficient measurement accuracy, but are in the middle of the rankings regarding the other requirements. The measurement-supported simulation techniques (section 2.6) score with high reliability, low susceptibility to loads and environment, low costs and low complexity and reasonable uncertainties under ideal conditions.

Acknowledgements

Financial support from the German Federal Ministry for the Environment, Nature Conservation and Nuclear Safety (contract ZIII5-16UM0068) and the European Union (contracts 019830 and 219110) are gratefully acknowledged. We also thank Olaf Bender, Janina Nettlau, Markus Pfänder, Jan-Peter Säck, Tamara Schapitz, Björn Schiricke, Reiner Schlee, and Ralf Uhlig for their valuable contributions.

References

[1] R. Monterreal, A. Neumann, Advanced flux measurement system for solar tower plants. Proc. of Seventh Intern. Symposium on Solar Thermal Concentrating Technologies, Moscow, Sept 26-30 (1994).

[2] E. Lüpfert, P. Heller, Steffen Ulmer, R. Monterreal, J. Fernández, Concentrated solar radiation measurement with video image processing and online fluxgage calibration. Solar Thermal 2000 International Conference Sydney, Australia, March 8-10 (2000).

[3] S. Ulmer, (2004). Messung der Strahlungsflussdichte-Verteilung von punktkonzentrierenden solarthermischen Kraftwerken, Fortschritt-Berichte Reihe 6, Nr. 510, VDI Verlag.

[4] S. Ulmer, E. Lüpfert, M. Pfänder, R. Buck, Calibration corrections of solar tower flux density measurements. Energy, 29, 5-6 (2004) 925-933.

[5] F. Göhring, O. Bender, M. Röger, J. Nettlau, P. Schwarzbözl, Flux density measurement on open volumetric receivers. Proceedings of SolarPACES 2011, Granada, Spain, Sept. 20-23 (2011).

[6] J. Pacheco, R. Houser, A. Neumann, Concepts to measure flux and temperature for external central receivers. Joint Solar Engineering Conference, ASME (1994) 595-603.

[7] J. Ballestrín, R. Monterreal, Hybrid heat flux measurement system for solar central receiver evaluation. Energy 29, 5-6 (2004) 915-924.

[8] R. Osuna, R, Morillo, J. M. Jiménez, V. Fernández-Quero, Control and operation strategies in PS10 solar plant. Proceedings 13th Solar PACES, Sevilla, Spain, June 20-23 (2006).

[9] B. Belhomme, R. Pitz-Paal, P. Schwarzbözl, S. Ulmer, New fast ray tracing tool for high-precision simulation of heliostat fields. Journal of Solar Energy Engineering, 131, 3 (2009).

[10] A. Neumann, A. Witzke, S. Jones, G. Schmitt, Representative terrestrial solar brightness profiles. Journal of Solar Energy Engineering, 124 (2002).